JOURNAL OF GEOPHYSICAL RESEARCH: SPACE PHYSICS, VOL. 118, 4946–4951, doi:10.1002/jgra.50464, 2013

Statistical analysis of EMIC waves in plasmaspheric plumes from Cluster observations

M. E. Usanova,[1] F. Darrouzet,[2] I. R. Mann,[1] and J. Bortnik[3,4]

Received 27 April 2013; revised 18 July 2013; accepted 19 July 2013; published 9 August 2013.

[1] Recently, electromagnetic ion cyclotron (EMIC) wave generation in plasmaspheric plumes has been the subject of extensive discussion. Theory predicts that regions of detached cold, dense plasma immersed in relatively low background magnetic field should aid EMIC wave growth and may provide conditions for interaction between the EMIC waves and relativistic (MeV) electrons, leading to energetic particle loss into the atmosphere. Since plasmaspheric plumes are specific to disturbed geomagnetic conditions, the link between EMIC waves and plumes may be especially important for radiation belt dynamics during magnetic storms. In this work, we present an in situ survey of EMIC waves in plasmaspheric plumes using data from the Cluster satellites and will address the question of whether plumes are important for EMIC wave generation from a statistical perspective. We used a survey of plasmaspheric plumes between 2001 and 2006 identified from the Waves of High frequency and Sounder for Probing of Electron density by Relaxation (WHISPER) sounder measurements. We further identified EMIC waves from simultaneous (with WHISPER) magnetic field measurements by the fluxgate magnetometer instruments and investigated the relationship between these two data sets. Only 10% of the time when Cluster-observed plumes along its orbit did we also observe EMIC waves. The wave occurrence outside plumes is further significantly reduced and is ~20 times lower in immediately adjacent regions than inside plumes. We found that cold plasma density was not a good predictor of EMIC occurrence inside the plumes and that the absolute density does not affect the EMIC probability. On the other hand, enhanced solar wind dynamic pressure significantly increases EMIC wave occurrence rate inside the plumes.

Citation: Usanova, M. E., F. Darrouzet, I. R. Mann, and J. Bortnik (2013), Statistical analysis of EMIC waves in plasmaspheric plumes from Cluster observations, *J. Geophys. Res. Space Physics*, *118*, 4946–4951, doi:10.1002/jgra.50464.

1. Introduction

[2] Electromagnetic ion cyclotron (EMIC) waves are transverse plasma waves generated in the magnetosphere by ring current protons with a temperature anisotropy ($T_{perp} > T_{par}$) and are typically registered in space and on the ground in the frequency range of 0.1–5 Hz. Early theoretical studies, further supported by observations, have shown that the EMIC wave growth leads to both the isotropization of the initially unstable proton distribution and the consequent pitch angle scattering and loss of particles into the dense upper atmosphere [see, e.g., *Cornwall*, 1965; *Søraas et al*., 1980; *Yahnin and Yahnina*, 2007].

[3] More recent theoretical studies [e.g., *Summers and Thorne*, 2003] have shown that in the inner magnetosphere, a resonant interaction with EMIC waves may also be important for MeV electron loss from the radiation belts, especially in regions of high plasma density and low magnetic field, such as plasmaspheric plumes and outer regions of the quiet time plasmasphere. So far, there has been limited direct experimental evidence supporting this hypothesis [see, e.g., *Miyoshi et al*., 2008], although there is some evidence from high-altitude stratospheric balloons measuring bremsstrahlung X-rays from precipitating electrons [*Foat et al*., 1998; *Millan et al*., 2002, 2011]. Nevertheless, EMIC waves may be potentially important not only for ring current loss but also for radiation belt dynamics.

[4] Early studies identified the plasmapause as a preferred region for EMIC wave generation, since increased plasma density lowers the EMIC instability threshold [e.g., *Gary and Lee*, 1994] and leads to a drastic enhancement in the convective EMIC wave growth rate [e.g., *Gendrin*, 1975]. However, later, it was found that the plasmapause is not a preferred region for EMIC wave generation [*Fraser and Nguyen*, 2001] and that EMIC waves are most frequently observed in the subsolar magnetosphere, close to the magnetopause where energetic ion distributions may become unstable to EMIC wave growth

[1]Department of Physics, University of Alberta, Edmonton, Alberta, Canada.
[2]Belgian Institute for Space Aeronomy, Brussels, Belgium.
[3]Center for Solar-Terrestrial Research, New Jersey Institute of Technology, Newark, New Jersey, USA.
[4]Department of Atmospheric and Oceanic Sciences, University of California, Los Angeles, California, USA.

Corresponding author: M. E. Usanova, Department of Physics, University of Alberta, CCIS, Edmonton, AB T6G 2E1, Canada. (musanova@ualberta.ca)

2169-9380/13/10.1002/jgra.50464

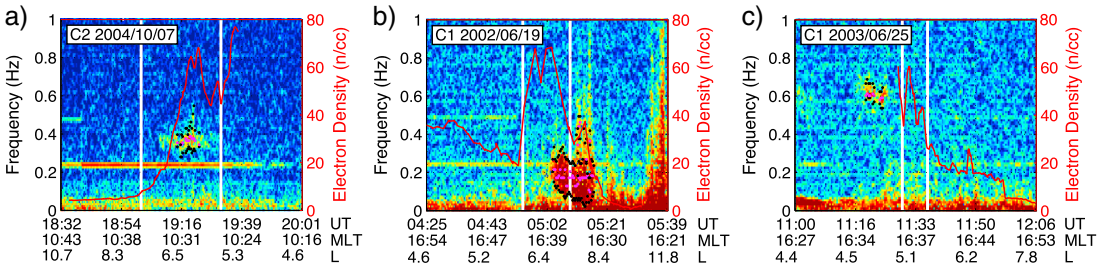

Figure 1. Spectrograms of the perpendicular component of magnetic field showing the EMIC wave location with respect to the plume: (a) inside, (b) spanning both inside and outside, and (c) outside. White vertical lines show the plume boundaries. The black and the purple dots define the EMIC bandwidth and the maximum power, respectively. The WHISPER electron density is plotted on top of the spectrograms by the red lines (where available).

during magnetospheric compressions [*Olson and Lee*, 1983; *Anderson et al*., 1992; *Anderson and Hamilton*, 1993]. A number of statistical studies have shown that the probability of EMIC wave observation increases with L-shell [*Anderson et al*., 1992; *Denton et al*., 2002], especially during intervals of enhanced solar wind dynamic pressure [*Usanova et al*., 2008; *McCollough et al*., 2010; *Usanova et al*., 2012].

[5] EMIC waves have also been observed in plasmaspheric plumes—regions of the outer plasmasphere transported sunward during magnetically disturbed times (see, e.g., case studies by *Fraser et al*. [2005], *Morley et al*. [2009], and *Yuan et al*. [2010]). However, from a statistical perspective, a link between EMIC waves and plasmaspheric plumes has not been definitively established. For example, *Posch et al*. [2010] compared EMIC wave occurrence on the ground at Antarctic high-latitude ($L = 6.28$–8.07) magnetometer stations and conjugate geosynchronous cold plasma densities between 1996 and 2003 and found a weak correspondence between EMIC waves and either plasmaspheric plumes or intervals when dense plasmaspheric plasma extended to geosynchronous orbit. They concluded that even though at times EMIC waves did coincide with intervals of plume occurrence, plumes were not necessary for EMIC wave generation around geosynchronous orbit, even during storm times. Their events were observed most often in association with increases in solar wind dynamic pressure.

[6] In this work, we investigate the relative importance of enhancements in plasma density and solar wind dynamic pressure (magnetospheric compression) in EMIC wave excitation by studying EMIC wave occurrence in plasmaspheric plumes. To the best of our knowledge, this is the first in situ statistical study examining the relationship between EMIC waves and plasmaspheric plumes globally, in a wide range of L-shells and at all magnetic local time (MLT) sectors.

2. Cluster Instrumentation and Survey Parameters

[7] For this study, we used data from four Cluster satellites carrying identical instrumentation [*Escoubet et al*., 1997]. They are positioned in a tetrahedral configuration with a separation distance that typically varies with time across the mission, from 100 km to a few Earth radii (R_E). The spacecraft follow similar polar orbits, with a period of approximately 57 h, an apogee of ~19.6 R_E, and a perigee of about 4 R_E. As the Cluster orbit precesses, all magnetic local times are covered by the spacecraft in the course of the year.

2.1. Plume Identification

[8] We based our EMIC study on a plasmaspheric plume survey by *Darrouzet et al*. [2008]. These authors routinely identified 782 plume crossings by the Cluster satellites from February 2001 through February 2006 using the Waves of High frequency and Sounder for Probing of Electron density by Relaxation (WHISPER) instrument [*Décréau et al*., 1997]. We further extended the original data set until the end of 2006, which resulted in a total of 993 plume crossings.

[9] WHISPER measures high-frequency electric fields in a range between 2 and 80 kHz and allows the estimation of electron plasma density n_e from the electron plasma frequency f_{pe} using the equation $f_{pe}(\mathrm{kHz}) = 9\sqrt{n_e(\mathrm{cm}^{-3})}$. Due to the upper frequency limit, the maximum electron density that can be resolved by WHISPER is ~80 cm^{-3}. Therefore, higher-density plumes cannot be accurately pinpointed with this instrumentation.

[10] Plasmaspheric plumes were identified by *Darrouzet et al*. [2008] based on a localized density increase (of ≥10 cm^{-3}) followed by a density decrease from the background value, adjacent to the main plasmasphere crossing. They also put a restriction on a minimum L-width of the increased density region, which should be at least 0.2 R_E wide to be considered as a plume.

[11] This data set contains events mostly for low and moderate geomagnetic activity ($Kp \leq 7$ and $Dst > -110$ nT). During highly disturbed geomagnetic conditions, the plasmasphere becomes eroded, and the plasmapause moves close to the Earth, below the Cluster perigee (4 R_E), and therefore, identification of a plume based on the above definition becomes more complicated.

[12] *Darrouzet et al*. [2008] outlined the following plume characteristics from their database. Plasmaspheric plumes were observed mainly in the afternoon and premidnight MLT sectors. The plumes had all possible density variations (below ~80 cm^{-3} being the WHISPER limit) and had no preferred density value. Most plumes had a width below 1.5 R_E, and on average, Cluster spent ~15 min crossing them. Lower-L (and also denser) plumes were seen in all MLT sectors, while less dense plumes extending farther out were observed only in the 10–18 MLT sector.

2.2. EMIC Wave Detection

[13] EMIC waves were identified from Cluster fluxgate magnetometer (FGM) [see *Balogh et al*., 2001] measurements.

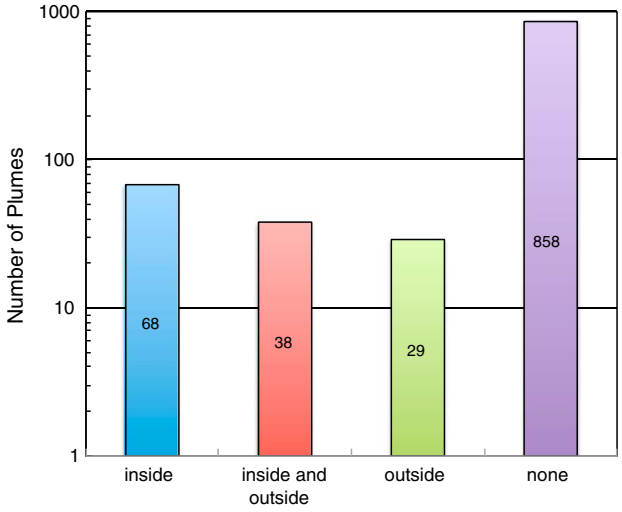

Figure 2. Distribution of EMIC wave location with respect to the plume. Note the logarithmic scale on the *y* axis.

The Cluster FGM provides measurements of the magnetic field in the frequency range from DC to ~10 Hz (32 Hz in burst mode) and sensitivity of at least 0.1 nT.

[14] We analyzed magnetic field data for each plume crossing from our survey, focusing on the interval [t_{in} − 30 min; t_{out} + 30 min], where t_{in} and t_{out} are the times of inward and outward plume crossings, respectively. First, we transformed the FGM data from GSM into local field-aligned coordinates (FAC), following the method described in *Rae et al*. [2005]. In FAC, the azimuthal direction is perpendicular to both the direction of the background magnetic field and the radial direction, which is defined by the vector from the center of the Earth to the satellite. Second, we used the sliding window fast Fourier transform to obtain spectral power of the perpendicular (azimuthal) magnetic field component and applied an automated wave detection algorithm [*Bortnik et al*., 2007], which selects spectral peaks that stand out (at least one magnitude greater in spectral power) above the background noise. In our case, we have chosen the window to be 2048 samples (93 s) long, with an overlap of ~30% (31 s), resulting in a ~60 s spacing between neighboring data blocks. The algorithm returns three recorded frequencies for detected emissions: a lower frequency, an upper frequency, and a frequency of maximum power, which are shown in Figure 1, superposed over spectrograms of the azimuthal magnetic field component. The black and the purple dots in this figure define the EMIC bandwidth and the maximum power, respectively. Also, Figure 1 shows three examples of EMIC waves and their location with respect to the plume. The white vertical bars denote the plume boundaries, and the red line superimposed over each spectrogram indicates the WHISPER electron density.

3. Analysis

3.1. EMIC Wave Occurrence in Plasmaspheric Plumes

[15] EMIC waves were observed during 106 (11%) out of 993 plume crossings: 68 (7%) inside and 38 (4%) spanning both inside and outside (as shown in Figures 1a and 1b, respectively). During 29 (3%) of the plume crossings, EMIC waves were observed outside of the plume within 30 min intervals preceding or following the plume encounter (Figure 1c). This occurrence distribution of EMIC wave event location with respect to the plume is shown in Figure 2 on a logarithmic scale.

[16] To investigate the occurrence rates of EMIC waves inside and outside plumes, we normalized the intervals of detected EMIC waves by the Cluster dwell time inside and immediately (±30 min) outside the plumes. We considered only the intervals when Cluster was at geocentric distances between 5 and 10 R_E and excluded the midnight-to-early-morning sector since EMIC probability has been shown to be very low there. We found that the EMIC wave occurrence inside the plumes was ~20 times higher than that immediately outside the plumes (during a 30 min interval adjacent to the plume crossing).

[17] We examined whether EMIC waves are preferentially generated on (or closer to) the duskside plume boundary, consistent with westward ion drift in the magnetosphere and theoretical predictions. We identified the MLT of the midpoint of EMIC wave activity region and examined its proximity to the westward and eastward plume boundaries. Though, in some cases, EMIC waves were indeed seen closer to the duskside plume crossing, on average, the EMIC wave region center was located at the plume center (not shown).

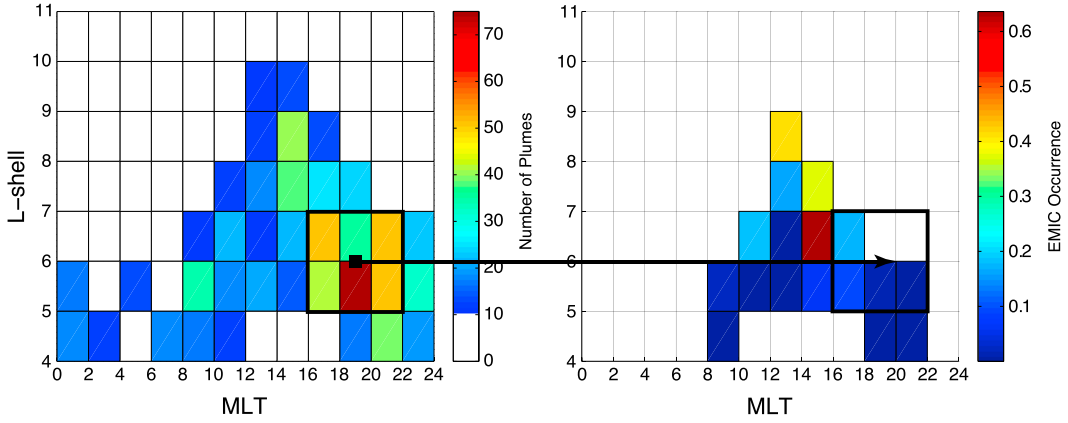

Figure 3. (left) *L*/MLT distribution of plasmaspheric plumes. (right) *L*/MLT EMIC wave occurrence rate in plumes. The black rectangle shows the region with maximum plume number. Bins with less than 10 plume crossings are not colored.

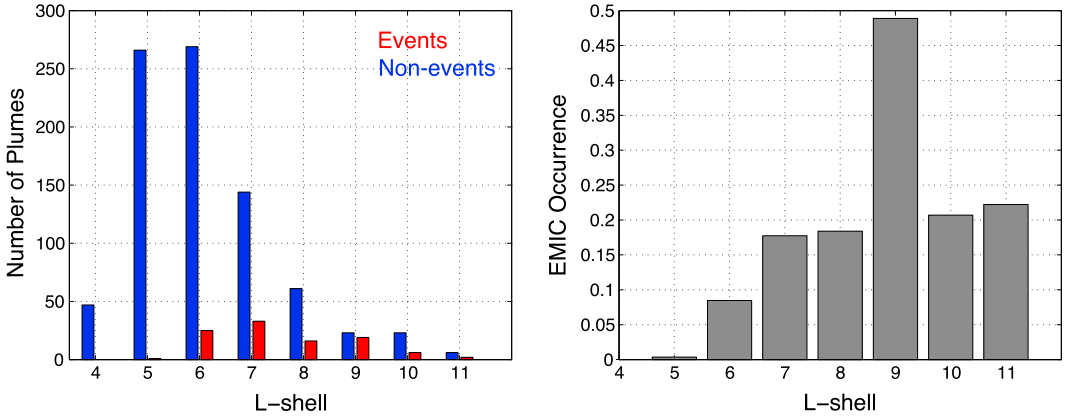

Figure 4. (left) Number of events (red) and nonevents (blue) and (right) EMIC wave occurrence rate in plumes as a function of L-shell.

[18] This observation is consistent with the hypothesis that small-scale cold plasma structures within a plume [see, e.g., *Moldwin et al*., 1995] might be important for EMIC wave generation. *Chen et al*. [2009, 2010] modeled the EMIC wave excitation in the presence of plumes. They found that in the case of a wide unstructured plume, the maximal wave gain is expected at the outer edge of the plume. However, for narrow plumes, the modeling predicts wave generation within the plume. Generation of cyclotron waves on small-scale cold plasma structures within the plume has also been discussed by *Yahnin et al*. [2006] and *Yuan et al*. [2012] on the basis of observations of the energetic proton and electron precipitation.

[19] Further, we investigated the L/MLT dependence of EMIC wave occurrence in plumes. We binned our data at 1 R_E in L and 2 h resolution in MLT and plotted the number of plume crossings as a function of L and MLT (Figure 3, left). The number of plume crossings in each bin is shown in the color bar (where the white color denotes less than 10 plume crossings). For each bin, we also computed the occurrence rate of EMIC waves in plumes by calculating the ratio of plume crossings during which EMIC waves were observed (either inside or inside and outside of the plume; here and after, we will refer to this as an EMIC plume "event") to the total number of plume crossings observed in this bin (Figure 3, right). A nonzero EMIC probability is seen at 8–22 MLT and $L = 5$–6 and narrows in MLT toward high L-shells. EMIC occurrence in plumes generally increases with L-shell; however, in most bins, it does not exceed 10%.

[20] The majority of plumes are observed in the duskside sector between $L = 5$–7 and MLT = 16–22, where the average number of plume crossings in each bin exceeds 40 (Figure 3, outlined box in the right and left panels). Even though the sample size is sufficiently large so as to be statistically significant, increased EMIC occurrence is not seen in this sector where the plume occurrence dominates.

[21] The left and right panels in Figure 4 show the number of EMIC events and nonevents and the EMIC wave event occurrence rate in plumes, respectively, as a function of L, averaged over all MLT sectors. Consistent with conclusions by *Usanova et al*. [2012], this figure demonstrates that EMIC occurrence at low L-shells (below geosynchronous orbit) is diminished. EMIC waves are not observed at $L < 5$ despite the fact that many plumes are observed at these L-shells. The probability of EMIC wave occurrence in plumes increases toward the magnetopause, where it reaches ~20%, also consistent with the observations on Active Magnetospheric Particle Tracer Explorers/Charge Composition Explorer [*Anderson et al*., 1992].

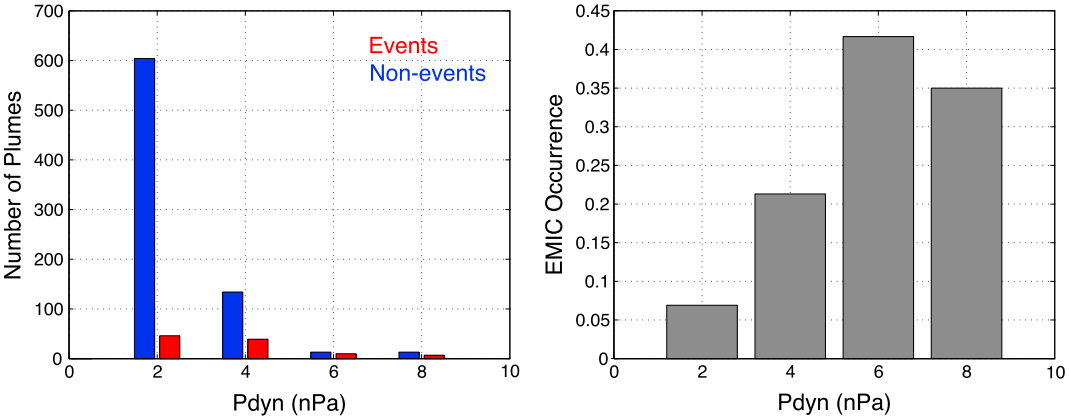

Figure 5. (left) Number of events (red) and nonevents (blue) and (right) EMIC wave occurrence rate in plumes as a function of solar wind dynamic pressure.

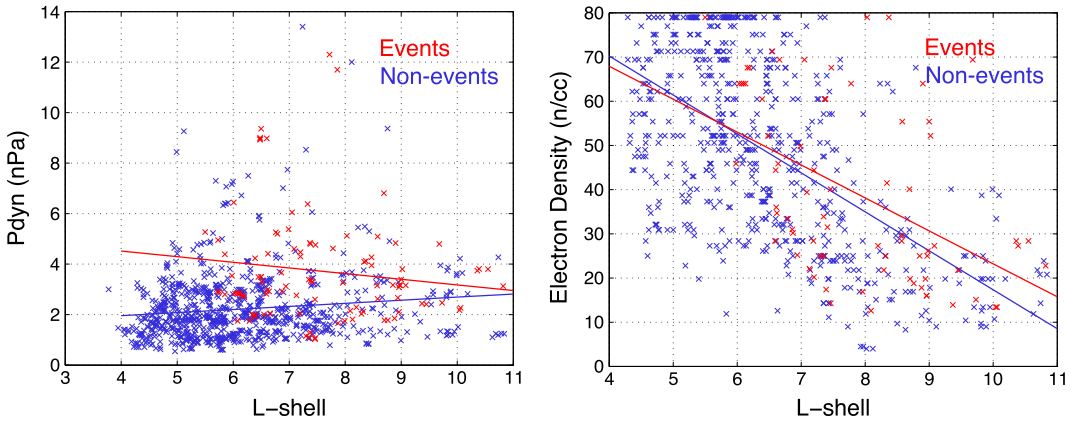

Figure 6. (left) Solar wind dynamic pressure and (right) electron density and as a function of L-shell and linear regression lines for EMIC events (red) and nonevents (blue).

[22] Since previous studies [e.g., *Usanova et al*., 2012, and references therein] outlined the importance of high solar wind dynamic pressure for the generation of ion temperature anisotropy and the consequent excitation of EMIC waves, we also examined the effect of solar wind pressure on EMIC wave occurrence in plumes. Similar to Figure 4, the left and right panels in Figure 5 show the number of events (red bars) and nonevents (blue bars) and the EMIC wave event occurrence in plumes, respectively, as a function of P_{dyn}. It is clear that the ratio between events and nonevents (Figure 5, left) and the probability of EMIC waves in plumes (Figure 5, right) drastically increases during intervals of enhanced solar wind dynamic pressure.

3.2. Difference Between Events and Nonevents

[23] For each individual plume crossing, we plotted the maximum value of electron density observed along one plume transit (Figure 6, right) and the value of solar wind dynamic pressure (Figure 6, left) at the time when the maximum electron density was observed, as a function of L-shell. Similar to the previous plots, we considered these dependencies for nonevents (blue) and events (red). For each set, we calculated a linear regression line, which is plotted on top. As shown in Figure 6 (right), despite the large statistical dispersion, in general, the difference in electron density between events and nonevents is insignificant, being 54 ± 31 and 63 ± 29 cm^{-3}, respectively. Both events and nonevents have peak plume densities which decrease with L, but show little dependence on electron density. At the same time, the average dynamic pressure during events is 1.7 times higher than during nonevents, being 3.7 ± 2.2 and 2.2 ± 1.3 nPa, respectively. This difference in dynamic pressure is more pronounced for the events observed at low L-shells and becomes smaller toward the magnetopause (at high L-shells), where plasma is often marginally stable and even small enhancements in solar wind dynamic pressure may lead to generation of EMIC waves [e.g., *Anderson and Hamilton*, 1993].

[24] We also examined the *Dst* and *Kp* indices during the events and nonevents and did not find a significant difference between them. Also, we did not find evidence that low-L events occurred during more disturbed geomagnetic conditions (higher *Kp*) than high-L events.

4. Summary and Conclusions

[25] We analyzed 993 plasmaspheric plume crossings by Cluster between 2001 and 2006 identified from WHISPER electron density measurements by *Darrouzet et al*. [2008]. We identified EMIC waves within and close to the plumes from simultaneous magnetic field measurements by Cluster FGM. Overall, EMIC waves were observed during 135 out of 993 plume crossings (14%)—either outside within a 30 min interval adjacent to the plume, inside, or spanning both outside and inside the plume. During 10% of plume crossings, EMIC waves were observed either inside the plume or at the plume boundary (inside and outside).

[26] We normalized the EMIC wave occurrence times inside and outside the plumes by Cluster dwell time in these regions to get the EMIC occurrence rate and found that EMIC waves are seen ~20 times more often inside the plumes than immediately outside the plumes, as defined by examining the 30 min intervals of Cluster orbit adjacent to the plume.

[27] The L/MLT distribution of EMIC events in plumes has a maximum at MLT = 12–16 beyond the geosynchronous orbit, which is consistent with earlier studies of EMIC wave occurrence [see *Anderson et al*., 1992; *Usanova et al*., 2012]. However, the $L = 5$–7/MLT = 16–22 region where the majority of plumes were observed did not exhibit enhanced EMIC occurrence. Also, we did not find evidence that EMIC waves were preferentially excited on the westward plume edge. On average, they were located equidistant from the duskside and dawnside plume boundaries.

[28] Finally, we examined the difference between plumes that produced EMIC waves (events) and plumes that did not (nonevents). The difference in electron plasma density between events and nonevents was not significant. Meanwhile, the average solar wind dynamic pressure during the events was 1.7 times as high as during the nonevents. Together with the enhanced EMIC wave probability at high L-shells in the dayside magnetosphere, this led us to conclude that solar wind dynamic pressure controls EMIC occurrence and that enhanced plasma density by itself is not sufficient for EMIC wave generation inside the plumes.

[29] **Acknowledgments.** We would like to acknowledge the Cluster FGM team and ESA Cluster Active Archive for providing magnetic field data. This work was supported in part by participation in the MAARBLE (Monitoring, Analyzing and Assessing Radiation Belt Loss and Energization) consortium. MAARBLE has received funding from the European Community's Seventh Framework Programme (FP7 SPACE 2010 1, SP1 Cooperation, Collaborative project) under grant agreement 284520. This paper reflects only the authors' views, and the European Union is not liable for any use that may be made of the information contained herein. MEU was partly supported by the Canadian Space Agency. IRM was supported by a Discovery Grant from Canadian NSERC. FD thanks the Belgian Federal Science Policy Office (BELSPO) through a Prodex project (contract 13127/98/NL/VJ). JB wishes to acknowledge NASA grant NNX11AD75G.

[30] Robert Lysak thanks the reviewers for their assistance in evaluating this paper.

References

Anderson, B. J., and D. J. Hamilton (1993), Electromagnetic ion cyclotron waves stimulated by modest magnetospheric compressions, *J. Geophys. Res.*, *98*(A7), 11,369–11,382, doi:10.1029/93JA00605.

Anderson, B. J., R. E. Erlandson, and L. J. Zanetti (1992), A statistical study of Pc 1–2 magnetic pulsations in the equatorial magnetosphere: 1. Equatorial occurrence distributions, *J. Geophys. Res.*, *97*(A3), 3075–3088, doi:10.1029/91JA02706.

Balogh, A., et al. (2001), The Cluster magnetic field investigation: Overview of in-flight performance and initial results, *Ann. Geophys.*, *19*, 1207–1217.

Bortnik, J., J. W. Cutler, C. Dunson, and T. E. Bleier (2007), An automatic wave detection algorithm applied to Pc1 pulsations, *J. Geophys. Res.*, *112*, A04204, doi:10.1029/2006JA011900.

Chen, L., R. M. Thorne, and R. B. Horne (2009), Simulation of EMIC wave excitation in a model magnetosphere including structured high-density plumes, *J. Geophys. Res.*, *114*, A07221, doi:10.1029/2009JA014204.

Chen, L., R. M. Thorne, V. K. Jordanova, C. P. Wang, M. Gkioulidou, L. Lyons, and R. B. Horne (2010), Global simulation of EMIC wave excitation during the 21 April 2001 storm from coupled RCM RAM HOTRAY modeling, *J. Geophys. Res.*, *115*, A07209, doi:10.1029/2009JA015075.

Cornwall, J. M. (1965), Cyclotron instabilities and electromagnetic emissions in the ultra low frequency and very low frequency ranges, *J. Geophys. Res.*, *70*(1), 61–69.

Darrouzet, F., J. De Keyser, P. M. E. Décréau, F. El Lemdani-Mazouz, and X. Vallières (2008), Statistical analysis of plasmaspheric plumes with Cluster/WHISPER observations, *Ann. Geophys.*, *26*(8), 2403–2417.

Décréau, P. M. E., et al. (1997), WHISPER, A resonance sounder and wave analyser: Performances and perspectives for the Cluster mission, *Space Sci. Rev.*, *79*, 157–193.

Denton, R. E., J. LaBelle, and X. Zhu (2002), Location of Pc 1–2 waves relative to the magnetopause, *Ann. Geophys.*, *20*, 1763–1767.

Escoubet, C. P., C. T. Russell, and R. Schmidt (Eds) (1997), *The Cluster and Phoenix Missions*, Kluwer Acad., Dordrecht, Netherlands.

Foat, J. E., R. P. Lin, D. M. Smith, F. Fenrich, R. Millan, I. Roth, K. R. Lorentzen, M. P. McCarthy, G. K. Parks, and J. P. Treilhou (1998), First detection of a terrestrial MeV X-ray burst, *Geophys. Res. Lett.*, *25*(22), 4109–4112.

Fraser, B. J., and T. S. Nguyen (2001), Is the plasmapause preferred source region of electromagnetic ion cyclotron waves in the magnetosphere?, *J. Atmos. Sol. Terr. Phys.*, *63*, 1225–1247.

Fraser, B. J., H. J. Singer, M. L. Adrian, D. L. Gallagher, and M. F. Thomsen (2005), The relationship between plasma density structure and EMIC waves at geosynchronous orbit, in *Inner Magnetosphere Interactions: New Perspectives From Imaging*, Geophys. Monogr. Ser., vol. *159*, edited by J. Burch, M. Schulz, and H. Spence, pp. 55–70, AGU, Washington, D. C., doi:10.1029/159GM04.

Gary, S. P., and M. A. Lee (1994), The ion cyclotron anisotropy instability and the inverse correlation between proton anisotropy and proton beta, *J. Geophys. Res.*, *99*(A6), 11,297–11,301, doi:10.1029/94JA00253.

Gendrin, R. (1975), Is the plasmapause a preferential region for proton precipitation?, *Ann. Geophys.*, *31*, 127–136.

McCollough, J. P., S. R. Elkington, M. E. Usanova, I. R. Mann, D. N. Baker, and Z. C. Kale (2010), Physical mechanisms of compressional EMIC wave growth, *J. Geophys. Res.*, *115*, A10214, doi:10.1029/2010JA015393.

Millan, R. M. (2011), Understanding relativistic electron losses with BARREL, *J. Atmos. Sol. Terr. Phys.*, *73*, 1425–1434, doi:10.1016/j.jastp.2011.01.006.

Millan, R. M., R. P. Lin, D. M. Smith, K. R. Lorentzen, and M. P. McCarthy (2002), X-ray observations of MeV electron precipitation with a balloon-borne germanium spectrometer, *Geophys. Res. Lett.*, *29*(24), 2194, doi:10.1029/2002GL015922.

Miyoshi, Y., K. Sakaguchi, K. Shiokawa, D. Evans, J. Albert, M. Connors, and V. Jordanova (2008), Precipitation of radiation belt electrons by EMIC waves, observed from ground and space, *Geophys. Res. Lett.*, *35*, L23101, doi:10.1029/2008GL035727.

Moldwin, M. B., M. F. Thomsen, S. J. Bame, D. McComas, and G. D. Reeves (1995), The fine-scale structure of the outer plasmasphere, *J. Geophys. Res.*, *100*(A5), 8021–8029, doi:10.1029/94JA03342.

Morley, S. K., S. T. Ables, M. D. Sciffer, and B. J. Fraser (2009), Multipoint observations of Pc1–2 waves in the afternoon sector, *J. Geophys. Res.*, *114*, A09205, doi:10.1029/2009JA014162.

Olson, J. V., and L. C. Lee (1983), Pc1 wave generation by sudden impulses, *Planet. Space Sci.*, *31*, 295–302.

Posch, J. L., M. J. Engebretson, M. T. Murphy, M. H. Denton, M. R. Lessard, and R. B. Horne (2010), Probing the relationship between electromagnetic ion cyclotron waves and plasmaspheric plumes near geosynchronous orbit, *J. Geophys. Res.*, *115*, A11205, doi:10.1029/2010JA015446.

Rae, I. J., et al. (2005), Evolution and characteristics of global Pc5 ULF waves during a high solar wind speed interval, *J. Geophys. Res.*, *110*, A12211, doi:10.1029/2005JA011007.

Søraas, F., J. A. Lundblad, N. F. Maltseva, V. Troitskaya, and V. Selivanov (1980), A comparison between simultaneous IPDP ground-based observations and observations of energetic protons obtained by satellites, *Planet. Space Sci.*, *28*(4), 387–405.

Summers, D., and R. M. Thorne (2003), Relativistic electron pitch-angle scattering by electromagnetic ion cyclotron waves during geomagnetic storms, *J. Geophys. Res.*, *108*(A4), 1143, doi:10.1029/2002JA009489.

Usanova, M. E., I. R. Mann, I. J. Rae, Z. C. Kale, V. Angelopoulos, J. W. Bonnell, K.-H. Glassmeier, H. U. Auster, and H. J. Singer (2008), Multipoint observations of magnetospheric compression-related EMIC Pc1 waves by THEMIS and CARISMA, *Geophys. Res. Lett.*, *35*, L17S25, doi:10.1029/2008GL034458.

Usanova, M. E., I. R. Mann, J. Bortnik, L. Shao, and V. Angelopoulos (2012), THEMIS observations of EMIC wave occurrence: Dependence on AE, SYMH, and solar wind dynamic pressure, *J. Geophys. Res.*, *117*, A10218, doi:10.1029/2012JA018049.

Yahnin, A. G., and T. A. Yahnina (2007), Energetic proton precipitation related to ion-cyclotron waves, *J. Atmos. Sol. Terr. Phys.*, *69*, 1690–1706.

Yahnin, A. G., T. A. Yahnina, and A. G. Demekhov (2006), Interrelation between localized energetic particle precipitation and cold plasma inhomogeneities in the magnetosphere, *Geomagn. Aeron.*, *46*, 332–338, doi:10.1134/S0016793206030078.

Yuan, Z., X. Deng, X. Lin, Y. Pang, M. Zhou, P. M. E. Décréau, J. G. Trotignon, E. Lucek, H. U. Frey, and J. Wang (2010), Link between EMIC waves in a plasmaspheric plume and a detached sub-auroral proton arc with observations of Cluster and IMAGE satellites, *Geophys. Res. Lett.*, *37*, L07108, doi:10.1029/2010GL042711.

Yuan, Z., Y. Xiong, D. Wang, M. Li, X. Deng, A. G. Yahnin, T. Raita, and J. Wang (2012), Characteristics of precipitating energetic ions/electrons associated with the wave-particle interaction in the plasmaspheric plume, *J. Geophys. Res.*, *117*, A08324, doi:10.1029/2012JA017783.